Chapter 16

Ultrashort Laser Pulses for Frequency Upconversion

Kun Huang, E Wu, Xiaorong Gu, Haifeng Pan and Heping Zeng

Additional information is available at the end of the chapter

http://dx.doi.org/10.5772/48541

1. Introduction

Single-photon frequency upconversion is a nonlinear process where the frequency of the signal photon is translated to the higher frequency with the complete preservation of all the quantum characteristics of the "flying" qubits [1,2]. One promising application of the single-photon frequency upconversion is converting the infrared photons to the desired spectral regime (usually visible regime) where the high performance detectors are available for sensitive detections [3-6]. The infrared single-photon frequency upconversion detection technique has been successfully used in a variety of applications, including infrared imaging [7] and infrared ultra-sensitive spectroscopy [8,9]. Additionally, such upconversion detector has greatly benefited the applications stringently requiring efficient photon detection in optical quantum computation and communication [10-12]. Furthermore, due to the phase-matching requirement in the frequency upconversion process, the upconversion detectors have some unique features, such as narrow-band wavelength acceptance [13] and polarization sensitivity [14], both of which render them very useful for fiber based quantum systems [15]. In the recent decade, experiments bear that the photon correlation, entanglement, and photon statistics are all well preserved in the coherent frequency upconversion [16-18].

Although the demonstration of frequency upconversion technology for strong light could be dated to the late 70s of last century [19], the single-photon frequency upconversion was just achieved at the beginning of this century [20]. The advent and rapid evolution of fabricating the periodically reversed nonlinear media led to the widespread use of quasi-phase matching (QPM), which has opened up new operating regimes for nonlinear interactions [21]. Rapidly growing interest has been focused in recent years on proposing novel schemes for achieving single-photon frequency upconversion with high efficiency and low noise and expanding its applications in all-optical nonlinear signal processing and in quantum state manipulation. With the help of extracavity enhancement, highly efficient up-conversion at single-photon level has been demonstrated by using bulk periodically poled lithium niobate (PPLN) crystals

[3]. By means of intracavity enhancement, a stable and efficient single-photon counting at 1.55 μm was achieved without the requirement of sensitive cavity servo feed-back [4,22]. Recently, frequency upconversion based on the PPLN waveguide attracts more and more attention [9,23]. All of the above single-photon frequency upconversion systems were pumped by the strong continuous wave (CW) lasers which would inevitably bring about severe background noise due to parasitic nonlinear interactions. Frequency upconversion based on pulsed pump arises to provide an effective solution [24]. To make sure that every signal photon can be interact with the pulsed pump field, synchronous pumping frequency upconversion system is thus introduced, which greatly improves the total detection efficiency. VanDevender *et al.* reported a frequency upconversion system based on electronic synchronization of the pump source and signal source with a repetition rate of just 40 kHz [5]. For satisfying applications of high-speed single-photon detection, fast and efficient single-photon frequency upconversion detection system operating at tens of MHz was realized based on the all-optical synchronized fiber lasers [25-27].

Thanks to the ultrashort optical pulses, intense peak power to obtain unit conversion efficiency could be achieved with a modest average pump power, thus loosening the restriction for the available output power from the pump laser [3,4]. Additionally, the background noise induced by the strong pump can be effectively reduced due to the pulsed excitation. Thus ultrashort pulses constitute ideal means as the pump source of frequency upconversion. The pulsed pumping system could not only permit efficient photon counting of infrared photons, but also quantum manipulation of single photons. One can realize a quantum state router by having a control on the multimode pump source [28]. Current researches also demonstrate simultaneous wavelength translation and amplitude modulation of single photons from a quantum dot by pulsed frequency upconversion [29]. Additionally, the concept of a quantum pulse gate is presented and an implementation is proposed based on spectrally engineered frequency upconversion [30].

In this chapter, we review the recent experimental progress in single-photon frequency upconversion with synchronous pulse pumping laser. The signal photons were tightly located within the synchronous pump pulses [25]. For improving the conversion efficiency, the specific control of the synchronized pulses was required, which led to the development of temporally and spectrally controlled single-photon frequency upconversion for pulsed radiation [26,27]. The compact fiber-laser synchronization system for fast and efficient single-photon frequency upconversion detection is of critical potential to stimulate promising applications, such as infrared photon-number-resolving detector (PNRD) [18,31] and ultrasensitive infrared imaging at few-photon level. This chapter is organized as follows. After this brief introduction, we present the basic theory for frequency upconversion in quantum frame in Section 2. Section 3 presents the experimental realization of synchronous pulsed pumping. Applications based on the synchronous pumping frequency upconversion system will be highlighted in Section 4 by the examples of infrared photon-number-resolving detection and several-photon-level infrared imaging. We conclude the chapter in Section 5 by emphasizing that the synchronous pumping frequency upconversion system will benefit numerous applications not only in infrared photon counting and also in manipulation of the quantum state of single photons.

2. Quantum description of frequency upconversion

Frequency upconversion based on sum frequency generation (SFG) is an optical process by which two optical fields combine in a quadratic nonlinear medium to generate a third field at a frequency equal to the sum of the two inputs as shown in Fig. 1. The theory of the SFG is well established for a long time and applied in a variety of classical and quantum optical applications. In this section, we go through the fundamental theory of SFG and derive the important results in quantum architecture. We investigate the quantum features according to different pumping methods for frequency upconversion, respectively. Specially, we will concentrate on the detailed discussion of the quantum characteristics in the multimode pumping scheme.

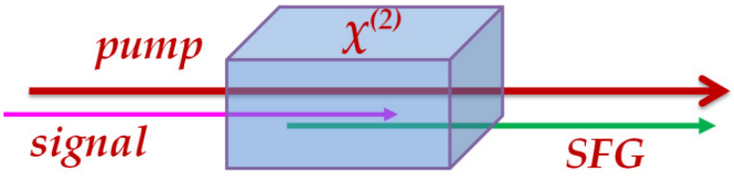

Figure 1. Schematic illustration of the frequency upconversion process.

2.1. Single-mode frequency upconversion

In quantum optics, the frequency upconversion is a nonlinear optical process, in which a photon at one frequency is annihilated and another photon at a higher frequency is created. We start with a Hamiltonian for three-wave mixing:

$$\hat{H}_{3W} = i\hbar g(\hat{a}_p \hat{a}_1 \hat{a}_2^{\dagger} - H.c.), \tag{1}$$

where $\hat{a}_1$ and $\hat{a}_p$ is the annihilation operators corresponding to the signal photon at ω_1 and pump photon ω_p, respectively. $\hat{a}_2^{\dagger}$ is the creation operator corresponding to the upconverted photon ω_2, g is the coupling constant which is determined by the second-order susceptibility of the nonlinear medium, and *H.c.* denotes a Hermitian conjugate. If the pump field is very strong with negligible depletion, as in the case here, we can classically treat it as a constant *Ep*. So the Hamiltonian in Eq. (1) becomes

$$\hat{H} = i\hbar g E_p(\hat{a}_1 \hat{a}_2^{\dagger} - H.c.). \tag{2}$$

Since for most cases, the upconverted frequency wave was in vacuum state at the input of the nonlinear medium. So the initial condition at the input facet of the nonlinear medium could be written as

$$|\Phi\rangle = |\Psi_1, 0_2\rangle, \tag{3}$$

where $|\Psi_1\rangle$ represents the input signal state and $|0_2\rangle$ represents the vacuum input of the SFG state. The dynamics of the input and output quantum fields in phase-matched SFG process can be described by the coupled-mode equations as

$$\hat{a}_1(L) = \hat{a}_1(0)\cos(|gE_p|L) - \hat{a}_2(0)\sin(|gE_p|L), \tag{4}$$

$$\hat{a}_2(L) = \hat{a}_2(0)\cos(|gE_p|L) + \hat{a}_1(0)\sin(|gE_p|L), \tag{5}$$

where L is the interaction length in the nonlinear crystal. The corresponding creation operators can be found by taking the Hermitian conjugates of these equations.

Eq. (5) indicates that frequency translation of any quantum state at ω_1 to the same quantum state at ω_2 with unity efficiency is possible, even at the single-photon level, if $|gE_p|L = \pi/2$. Note that the coherent quantum transduction from one frequency to a higher frequency would preserve complete coherence properties including entanglement, quantum correlation, and photon statistics.

At the output of the nonlinear medium, the average photon number of infrared signal can be calculated from expected value of the photon number operator:

$$\begin{aligned} N_1(L) &= \left\langle \hat{a}_1^{\dagger}(L)\hat{a}_1(L) \right\rangle \\ &= \left\langle \psi_1 \middle| \hat{n}_0 \middle| \psi_1 \right\rangle \cos^2(|gE_p|L) \\ &= N_1^0 \cos^2(|gE_p|L), \end{aligned} \tag{6}$$

where $\hat{n}_0$ denotes the photon number operator of the input infrared signal; N_1^0 is the average photon number of the input signal.

Meanwhile, the average number of the SFG photons can be likewise given by

$$N_2(L) = N_1^0 \sin^2(|gE_p|L). \tag{7}$$

From Eq. (6) and Eq. (7), the upconversion efficiency can be given as

$$\eta = \frac{N_2(L)}{N_1(0)} = \sin^2(|gE_p|L). \tag{8}$$

Additionally, we can get $N_2(L) + N_1(L) = N_1^0$, indicating the energy conservation during the conversion process. The correlation between the upconverted photons and unconverted photons is shown in Fig. 2.

The joint probability P_{12} of simultaneously detecting a photon at both ω_1 and ω_2 at the output of the frequency upconverter is proportional to $\left\langle \hat{n}_1\hat{n}_2 \right\rangle$. With the help of Eq. (4,5) we readily obtain that

$$\begin{aligned} \left\langle \hat{n}_1\hat{n}_2 \right\rangle &= \left\langle \hat{a}_1^{\dagger}(L)\hat{a}_2^{\dagger}(L)\hat{a}_2(L)\hat{a}_1(L) \right\rangle \\ &= [\left\langle \hat{n}_0^2 \right\rangle - \left\langle \hat{n}_0 \right\rangle]\cos^2(|gE_p|L)\sin^2(|gE_p|L). \end{aligned} \tag{9}$$

Inserting Eq. (8) into the above equation, we have

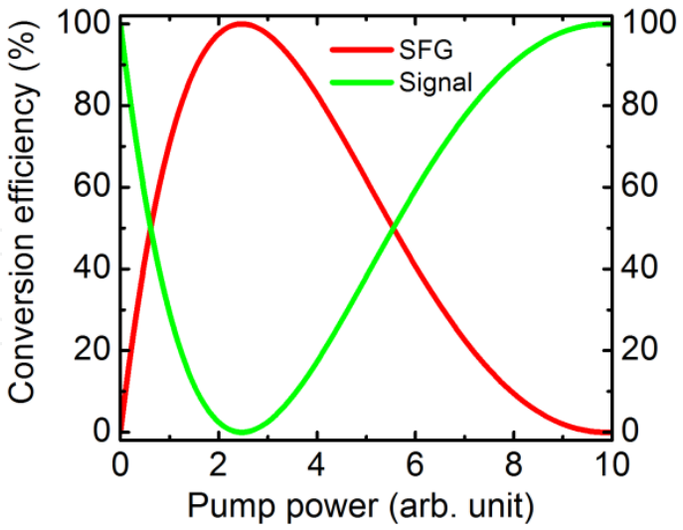

Figure 2. Correlation between the upconverted SFG photons and unconverted signal photons.

$$\langle \hat{n}_1 \hat{n}_2 \rangle = [\langle \hat{n}_0^2 \rangle - \langle \hat{n}_0 \rangle]\eta(1-\eta), \tag{10}$$

which is dependent on the conversion efficiency of the frequency upconversion process.

Moreover, the intensity cross-correlation function $g^{(2)}(\tau)$ at $\tau = 0$ is then obtained from

$$g^{(2)}(0) = \frac{\langle \hat{n}_1 \hat{n}_2 \rangle}{\langle \hat{n}_1 \rangle \langle \hat{n}_2 \rangle} = \frac{\langle \hat{n}_0^2 \rangle - \langle \hat{n}_0 \rangle}{\langle \hat{n}_0 \rangle^2}. \tag{11}$$

When input signal photons are in single photon state, meaning $\langle \hat{n}_0^2 \rangle = \langle \hat{n}_0 \rangle$, the probability of detecting a photon both in frequency ω_1 and ω_2 is then zero. The unconverted infrared photons and SFG photons are anti-correlated. When the incident photons are in a coherent state, meaning $\langle \hat{n}_0^2 \rangle - \langle \hat{n}_0 \rangle = \langle \hat{n}_0 \rangle^2$, the intensity cross-correlation equals to 1, which means no anti-correlation will be observed. It indicates that the frequency upconversion process is a random event for the individual incident signal photons.

All above results are obtained on the basis of perfect phase matching. The phase matching condition is sensitive in the SFG interaction due to the limit spectral bandwidth of the nonlinear medium. Taking into account the phase mismatching [32], the quantum state of the SFG photons can be expressed as

$$\begin{aligned} \hat{a}_1(L,\Delta\omega) = {} & \cos(qL)\exp(-i\Delta\omega\Delta kL/2)\hat{a}_1(0,\Delta\omega) \\ & -\frac{igE_p}{q}\sin(qL)\exp(-i\Delta\omega\Delta kL/2) \\ & \times[\frac{\Delta\omega\Delta k}{2gE_p}\hat{a}_1(0,\Delta\omega)+\hat{a}_2(0,\Delta\omega)], \end{aligned} \tag{12}$$

$$\begin{aligned}\hat{a}_2(L,\Delta\omega) &= \cos(qL)\exp(-i\Delta\omega\Delta kL/2)\hat{a}_2(0,\Delta\omega) \\ &+\frac{igE_p}{q}\sin(qL)\exp(-i\Delta\omega\Delta kL/2) \\ &\times[\frac{\Delta\omega\Delta k}{2gE_p}\hat{a}_2(0,\Delta\omega)+\hat{a}_1(0,\Delta\omega)],\end{aligned} \tag{13}$$

where Δk represents the phase-mismatch at frequency detuning $\Delta\omega$, and $q=[(gE_p)^2+(\Delta\omega\Delta k/2)^2]^{1/2}$. At zero detuning $(\Delta\omega=0)$, Eqs. (12) and (13) can be deduced to Eqs. (4) and (5), respectively. The unity single-photon frequency conversion can be achieved when $|gE_p|L=\pi/2$ is fulfilled. At nonzero detuning $(\Delta\omega\neq 0)$, although a similar condition $qL=\pi/2$ can be fulfilled, the perfect quantum conversion is impossible due to the disturbance of the vacuum state $\hat{a}_2(0,\Delta\omega)$. Therefore, for practical experiments, the spectral requirement of the pump field for frequency upconversion should be well concerned.

2.2. Synchronous pumping frequency upconversion

Could the complete quantum state transduction be feasible when the signal and the pump source were both in the multi-longitudinal modes? This is the instance of the synchronous pumping frequency upconversion system. Obviously, the frequency conversion process becomes more complicated due to the commutative nonlinear coupling of the pump modes and signal modes.

The Hamiltonian can be rewritten as

$$\hat{H}=i\hbar g\sum_{ij}E_{pi}(\hat{a}_{1j}\hat{a}_{2ij}^{\dagger}-H.c.), \tag{14}$$

where the E_{pi} is the pump electric field related to each longitudinal mode numbered by *i*, and the $\hat{a}_{1j}$ is the annihilation operator of the infrared signal photons related to each longitudinal mode numbered by *j*, the $\hat{a}_{2ij}^{\dagger}$ is the creation operator of the SFG photons corresponding to the longitudinal mode of both pump field and infrared signal photons. Then the dynamics of the input and output quantum fields in phase-matched SFG processes can be described by the coupled-mode equations as

$$\begin{aligned}\frac{d\hat{a}_{1j}}{dt} &= \frac{1}{ih}[\hat{a}_{1j},\hat{H}]=-g\sum_i E_{pi}\hat{a}_{2ij} \\ \frac{d\hat{a}_{2ij}}{dt} &= \frac{1}{ih}[\hat{a}_{2ij},\hat{H}]=gE_{pi}\hat{a}_{1j}.\end{aligned} \tag{15}$$

The superposition state of the infrared signal photons and SFG photons are represented by the operators $\hat{a}_1$, $\hat{a}_2$, which are defined as

$$\begin{aligned}\hat{a}_1 &= \sum_i \hat{a}_{1j} \\ \hat{a}_2 &= \sum_j\sum_i C_i\hat{a}_{2ij},\end{aligned} \tag{16}$$

where $E_p^2 = \sum_i E_{pi}^2$ and $C_i = E_{pi} / E_p$ denotes the probability amplitude of each longitudinal mode. Then the coupled-mode equation can be trivially solved by using the initial condition at the input facet of the nonlinear medium to yield

$$\hat{a}_1(L) = \hat{a}_1(0)\cos(|gE_p|L) - \hat{a}_2(0)\sin(|gE_p|L), \tag{17}$$

$$\hat{a}_2(L) = \hat{a}_2(0)\cos(|gE_p|L) + \hat{a}_1(0)\sin(|gE_p|L). \tag{18}$$

We get the same results as that in a single-longitudinal mode situation (Eqs. (4, 5)). When $|gE_p|L = \pi/2$ is satisfied, the coherence properties of the incident signal photons could be maintained during the upconversion process in this multi-mode system.

Here we can clearly see that either in single-mode regime or in multi-mode regime, the upconversion can, in principle, be used to transduce one photon at a given wavelength to another wavelength in preservation of all the quantum characteristics. Such quantum upconverter would not only be useful in the fields related to efficient infrared photon counting, but also helpful to implement novel quantum functions such as quantum interface and quantum gate or quantum shaper. In next section, experimental realization of the single-photon frequency upconversion with synchronously pumping will be demonstrated at length.

3. Experimental realization of single-photon frequency upconversion system

To achieve efficient and low-noise single-photon frequency upconversion system, various schemes have been proposed by the researchers for different applications in recent years. The upconversion technique typically requires a sufficiently strong pump to achieve unity nonlinear frequency conversion efficiency in a quadratic nonlinear crystal. The requisite strong pump can be achieved by using an external cavity or intracavity enhancement [3,4] or a waveguide confinement [9,23]. With such high intensity of pump, frequency up-conversion was implemented with almost 100% internal conversion efficiency. Nevertheless, a strong pump field inevitably brings about severe background noise because of parasitic nonlinear interactions, such as spontaneous parametric downconversion and Raman scattering. Pulsed pumping technique is given rise to circumscribe induced noise within the narrow temporal window of the pump pulses. Ultralow background counts of 150/s was reported with the help of a long-wavelength pump scheme [24]. In order to include every signal photon within the pump pulse for improving the total detection efficiency, researchers recently develop a coincidence single-photon frequency upconversion system [5,25-27]. In this section, we will focus on the synchronous pulsed pumping technique and its experimental results.

Fig. 3 shows the experimental setup of the synchronous single-photon frequency upconversion detection. The system was composed of a passive master-slave synchronization fiber-laser system and a single-photon frequency upconversion counting system. In the synchronization fiber-laser system, both two fiber lasers were passively mode-locked by the nonlinear polarization rotation in the fiber cavity, operating at the repetition rate of 17.6 MHz to

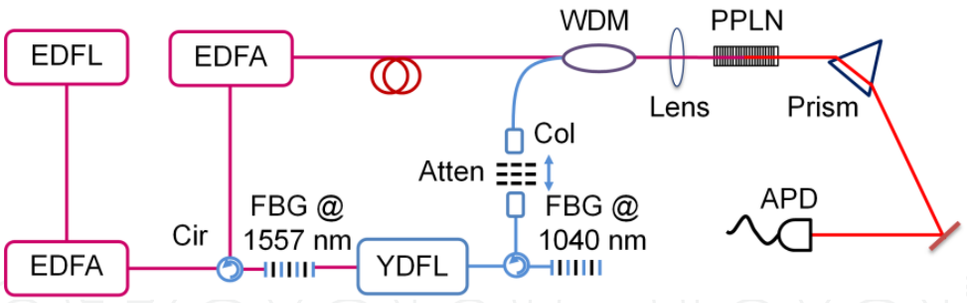

Figure 3. Experimental setup of the synchronous single-photon frequency upconversion detection. YDFL, ytterbium-doped fiber laser; EDFL, erbium-doped fiber laser; EDFA, erbium-doped fiber amplifier; Cir, circulator; Col, collimator; Atten, attenuator; WDM, wavelength-division multiplexer; FBG, fiber Bragg grating; PPLN, periodically poled lithium niobate crystal; APD, avalanche photodiodes.

satisfy the high-speed detection. The master laser was an Er-doped fiber ring laser. The ring cavity consisted with 1.5-m Er-doped fiber, standard single-mode fiber and dispersion-shifted fiber. By optimizing the lengths of the single-mode and dispersion-shifted fibers while maintaining the total cavity length, the dispersion in the cavity was well controlled. The spectrum of the output laser centered at 1563.8 nm with a full width at half maximum (FWHM) of 6.2 nm. A narrow spectral portion of the master laser was extracted by the FBG reflection for approaching the QPM bandwidth of the PPLN. This part was further amplified by an Er-doped fiber amplifier (EDFA) as the pump source. The maximum output power was about 60 mW and the output spectrum from the amplifier centered at 1557.6 nm with an FWHM of 0.56 nm [Fig. 4(a)]. The transmission from the FBG was injected as a seed to the slave laser cavity via a 1040/1557-nm wavelength-division multiplexer (WDM) to trigger the mode-locking of the Yb-doped fiber laser. An FBG was used as well at the slave laser output to control the spectral matching of the signal photons. The filtered spectrum was centered at 1040.0 nm with the bandwidth about 0.35 nm (FWHM) [Fig. 4(b)]. Injection-locking of the slave laser ensured the synchronization between the master and slave laser due to the fact that the transmission from the FBG shared exactly the same spectral mode separation with the reflection.

With this master-slave configuration, the two synchronized lasers could be isolated from each other, and thus free from mutual perturbation. This all-optical synchronization technique is superior to other passive synchronization methods due to its simplicity and robustness [33-35]. If self-started mode-locking existed in the slave laser, synchronized injection-locking could be obtained as well, but only within a sensitive slave cavity length match and could not last long, which would not be implemented in the frequency upconversion system. The self-started mode-locking would compete with the injection-triggered mode-locking, leading to the instability. To reduce the instability, self-started mode-locking was avoided in the slave fiber laser by properly adjusting the laser polarization state in the cavity. In such a critical position, the slave laser could only be mode-locked with the presence of the seed injection. The cavity length of the slave laser was adjusted to be the same as the master laser by carefully moving one of the fiber collimators on the stage. Eventually, the slave laser was synchronized with the master laser at the same

repetition rate. And the stability of synchronization was enhanced by optimizing the master laser injection polarization. With such setup, we achieved the maximum cavity mismatch tolerance of 25 μm with the long-term stability of several hours.

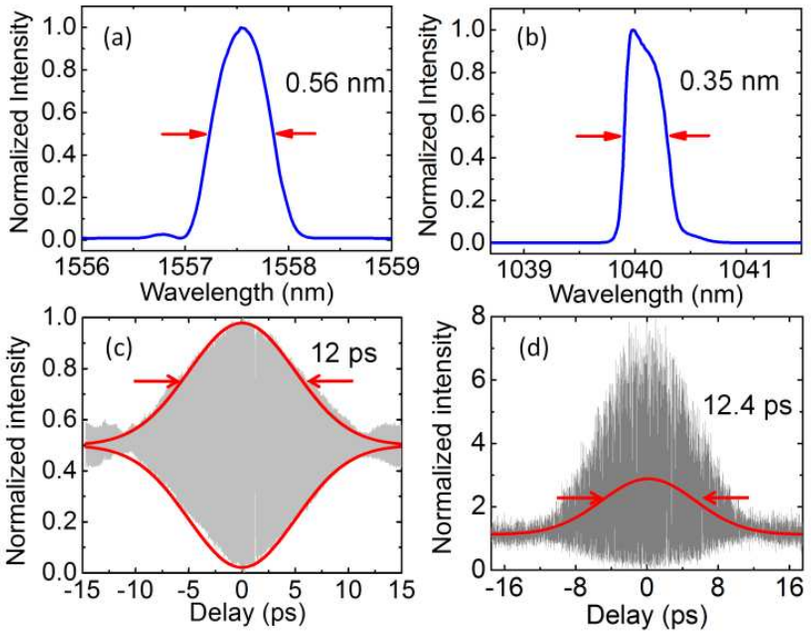

Figure 4. Spectrum of the pump source from the EDFL (a) and the signal source from the YDFL (b), respectively. Autocorrelation pulse profiles of the pump source (c) and the signal source from (d), respectively. Solid symbols are the experimental data and solid curves are the Gaussian fits to the data.

The signal pulse duration was measured by an autocorrelator with the FWHM bandwidth of 12 ps [Fig. 4(c)], corresponding to the actual pulse duration of 6 ps by taking the denominator of 2. In order to optimize the upconversion efficiency, the pump pulse duration relative to the signal pulse needs to be considered carefully [5]. The total conversion efficiency dependent on the pulse overlapping is given by

$$P_{overlap} = \int_{-\infty}^{+\infty} P_0(I_p(t)) I_s(t) dt, \tag{19}$$

where P_0 is the probability of upconversion dependent on pump intensity I_P as $\sin^2(I_p^{1/2})$, and $I_s(t)$ is the normalized input pulse profile

$$\int_{-\infty}^{+\infty} I_s(t) dt = 1. \tag{20}$$

The simulated conversion efficiency shown in Fig. 5 indicates that the total efficiency increases as the pump pulse duration goes longer by assuming a constant FWHM duration (6 ps) for the signal pulse. When the pump pulse duration is much shorter than the signal pulse, the conversion efficiency is quite low as most of the photons distribute outside of the pump pulse temporal window. On the other hand, too long pulse duration will lead to reduction of the energy utilization efficiency and increase of the background counts. Therefore, to achieve a conversion efficiency over 90% with experimentally available pump

intensity, it is theoretically necessary to make pulse duration ratio between the pump and signal slightly larger than 1.2.

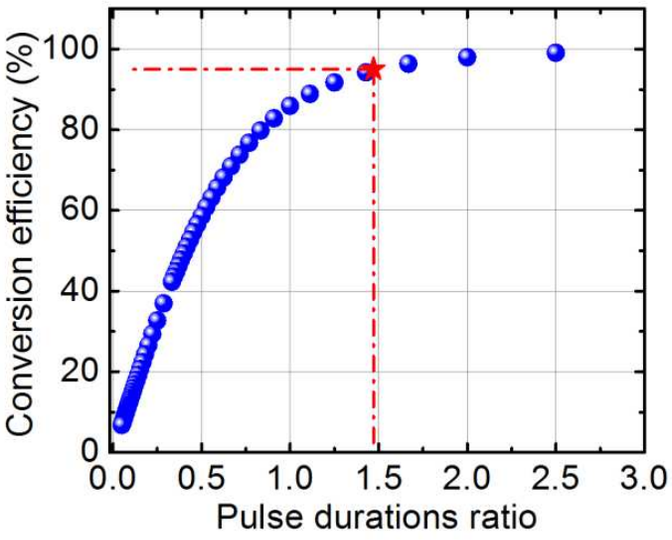

Figure 5. Simulated conversion efficiency as a function of the pulse duration ratio between the pump and signal. The red star indicates the experimental situation.

Thanks to the spectral filtering by the FBGs in the experiment, the pulse durations of the master and slave lasers were stretched according to the time-frequency Fourier transform. With the help of cavity dispersion management in the master laser cavity, the desired temporal match was achieved. The pump pulse duration was measured to be 8.8 ps [Fig. 4 (d)]. In this way, the signal photons and pump pulses were well matched temporally, guaranteeing an efficient upconversion with a relatively low background noise. According to the theoretical simulation, the conversion efficiency can reach 95% as shown by the red star in Fig. 5.

In the experiment, the timing jitter between the signal and pump pulses was measured to be as low as 45 fs shown in Fig. 6. Such a low timing jitter would impose a negligible influence on the temporal distribution of the signal photons within the pump pulse window. So the single-photon signal could be synchronously gated with a sufficiently high stability for coincidence upconversion detection.

As shown in Fig. 3, the signal beam and pump beam were then combine by a 1040/1557-nm WDM before being focused at the center of the 50-mm-long PPLN crystal. The temperature of the crystal was optimized at 130.4 °C for the grating period of 11.0 μm. The temperature was high enough to avoid photorefractive effects [36]. The infrared object beam interacted with the pump beam, and was upconverted through SFG to generate the visible photon at 624 nm.

For a single-photon frequency upconversion system, besides efficiency and stability, background noise was also a very important metrics for the detector performance. To analyze the noise, the spectrum before the filtering system was recorded. No observable peaks around the wavelength of the sum-frequency photons appeared when no signal photons were incident, revealing that the major noise from pump-induced parametric fluorescence was almost eliminated in our experiment. Considering the pulsed pump mode, the noise

was localized within a very short pump time window which was much shorter than any electronic gates applied on the APD, leading to a very low noise counts on the APD.

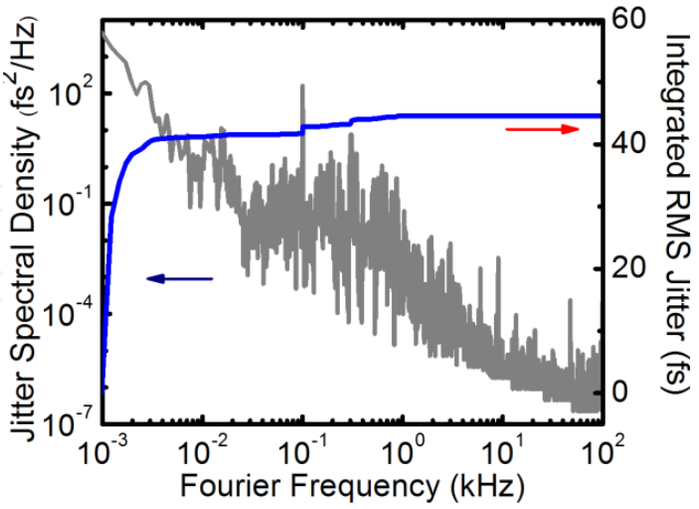

Figure 6. Timing jitter power spectral density and the integrated timing jitter in Fourier domain.

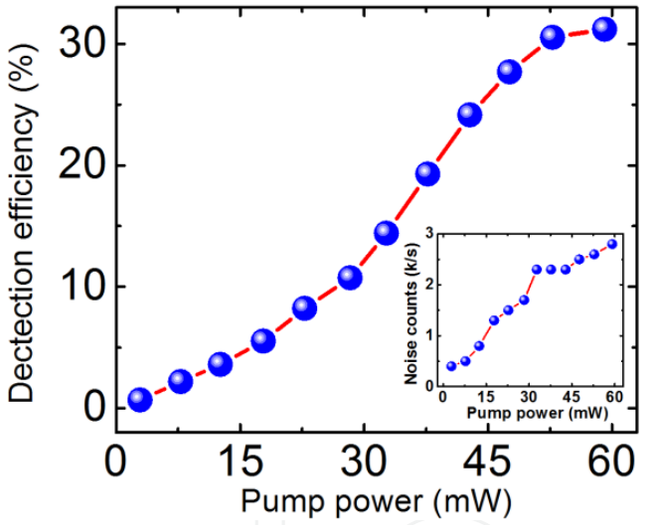

Figure 7. Conversion efficiency as a function of the pump power. Inset: background counts vs the pump power.

As a result, the maximum detection efficiency of 31.2% was achieved at the pump power of 59.1 mW, with the corresponding background counts of 2.8×10^3 s^{-1} shown in Fig. 7. The maximum conversion efficiency of the system was calculated to be 91.8% after taking into account the transmittance of the filters and the quantum efficiency of the Si-APD SPCM. Since the signal and pump pulses were focusing on PPLN crystal, the imperfection of the conversion efficiency might be mainly caused by the spatial mode mismatching of the pump and signal. Compared with the background counts of CW pumping (1×10^5 s^{-1}) [3,4], it was about two orders smaller in synchronously pulsed pumping scheme. As a figure of merit, we calculated the noise equivalent power (NEP = $h\upsilon(2R_{BC})^{1/2}/\eta$) divided by the operation rate f, where $h\upsilon$, R_{BC} and η are the energy of a signal photon, the background noise, and the detection efficiency, respectively. NEP/f was an important parameter of the sensitivity of an

optical detector, especially referring to the determinant of the data acquisition time in general and the key generation rate in quantum key distribution (QKD) systems [23]. At the peak detection efficiency, the NEP/f was as low as 2.6×10^{-24} W/Hz$^{3/2}$, thus showing that such scheme is suitable for the fast and efficient infrared single-photon detection.

The synchronous pumping single-photon frequency upconversion system is not only applied in the infrared photon detection with high efficiency and low background noise. More importantly, due to the unique quantum features in coherence preservation, it may stimulate promising applications with compact all-fiber devices in temporal and spectral control of single-photon nonlinear photonics. In Section 4, some applications are presented.

4. Applications in infrared PNRD and imaging

We believe that the compact fiber-laser synchronization system for fast and efficient single-photon frequency upconversion is of critical potential to stimulate other promising applications, such as high-speed QKD and quantum interface. The synchronous frequency upconversion system will also benefit infrared photon number resolving detection or few-photon-level infrared imaging.

4.1. Infrared photon-number-resolving detection

PNRD supports promising and important applications in few-photon detection, nonclassical photon statistics measurements, fundamental quantum optics experiments, and practical quantum information processing [37–39]. In the visible regime, PNRD with high quantum efficiency and low dark counts could be realized by employing silicon-based multipixel photon counter (Si-MPPC) [40]. Meanwhile at telecom wavelengths, PNRD could be achieved with InGaAs-based avalanche photodiodes (APD) operating in non-saturated mode [41]. However, PNRD for the wavelengths around 1 μm is still a bottleneck because both Si- and InGaAs-detectors are insensitive at those wavelengths. Recent advances in infrared photon detection technology show that coherent upconverison of quantum states is feasible, where the photon statistics would be conserved consequently [10,11]. Therefore, it is possible to count the visible replicas via frequency upconversion to realize PNRDs around 1 μm.

Based on coincidence frequency upconversion presented in Section 3, photon-number-resolving detection at 1.04 μm has been realized. The experimental setup was schematically illustrated in Fig. 8, consisting of two parts: synchronization fiber laser system for the pump pulses and signal photons, and photon-number-resolved detection system based on coincidence frequency upconversion and the Si-MPPC. The signal photons at 1.04 μm were then upconverted by the synchronized pump pulses at 1.55 μm in the PPLN crystal. Then the SFG photons passed through a group of filters before impinging on the Si-MPPC with a multimode fiber pigtail. The Si-MPPC (Hamamatsu Photonics S10362-11-100U) was composed of 10×10 APDs which were arranged on an effective active area of 1 mm^2 with a photon detection efficiency of 16.0% (including the fiber coupling efficiency). When the incident photons were injected onto different pixels, the output voltage of the superposition from all APD pixels was proportional to the number of incident photons [40]. The histogram

of the peak voltage from the output of Si-MPPC was showed in Fig. 9(a). The pulse area spectrum featured a series of peaks representing the different photon number states. By fitting each peak to Gaussian function, the probability distribution was obtained as shown in Fig. 9(b). The area under each Gaussian curve gave the number of events presenting that photon number state. The area of each peak could be normalized by the total area to give the probability distribution. As the input light was in coherent state, the upconverted photons statistics obeyed the Poissionian law. By fitting the experimental data according to Poisson distribution, we got the detected photon number of 4.65. With different incident photon flux, the photon numbers detected by SPCM were shown with circles in Fig. 9(c). Since SPCM could not discriminate more than one photon per shot, it was obviously saturated with large incident photon numbers. In contrast, as shown with squares in Fig. 9(c), the detected photon numbers of Si-MPPC linearly increased with the incident photon numbers. It showed that the Si-MPPC could correctly identify the photon numbers per pulse with a large dynamic range, which was promising in few-photon-level detection.

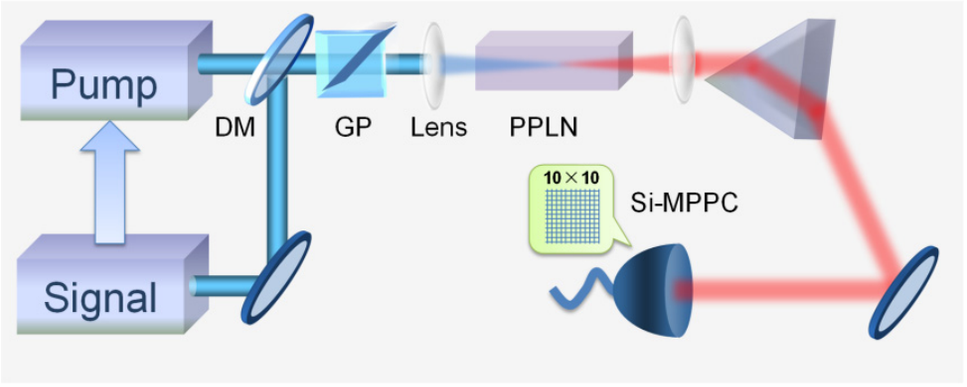

Figure 8. Experimental setup for the 1.04 μm photon-number-resolved detection. DM, dichroic mirror; GP, Glan prism; Si-MPPC, silicon multipixel photon counter.

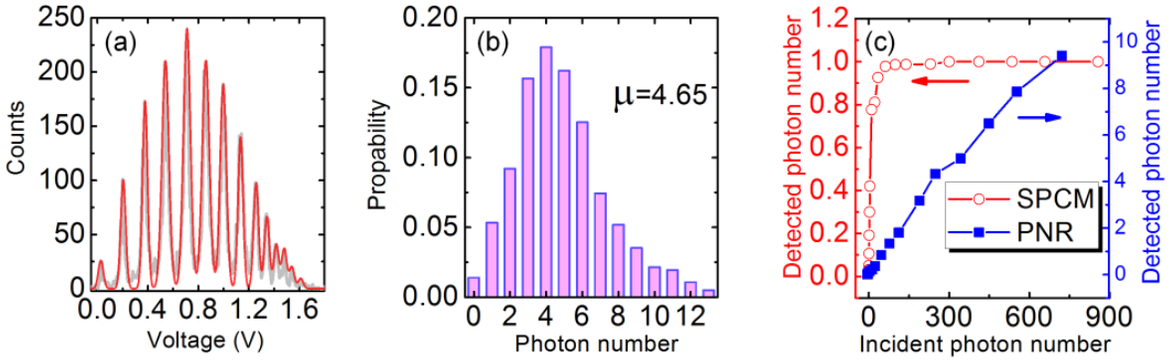

Figure 9. (Color online) (a) Output voltage amplitude histogram for the upconverted photons. (b) Photon number distribution. (c) Detected photon numbers by SPCM (circles) and Si-MPPC (squares) as a function of incident photon numbers.

The photon-number-resolving performance was improved by reducing the background counts with a synchronous pump as the coincidence gate and reducing the intrinsic parametric fluorescence influence with long-wavelength pumping. As a result, a total

detection efficiency of 3.7% was achieved with a quite low noise probability per pulse of 0.0002. Such a low background noise probability could remarkably improve the sensitivity of the frequency-upconversion PNRD. The remarkable decrease in background noise would optimize applications such as quantum entanglement and quantum teleportation [42] and improve the signal-to-noise ratio of widely used light detection and ranging system, since the background counts would randomly couple into the modes of the quantum states, which may significantly affect the original photon number distribution [38]. The approach may find promising applications in various quantum optical experiments using nonclassical light sources to demonstrate the features of quantum states around 1 μm [43].

4.2. Ultrasensitive infrared imaging

Realization of ultra-sensitive infrared imaging has critical importance for applications such as astronomy, medical diagnosis, night-vision technology and chemical sensing. Currently, the infrared imaging detectors are available, like the commonly used linear InGaAs photodiode array. However, suffering from the severe dark current, the sensitivity of such detectors is largely limited [44]. Even though liquid-nitrogen-cooling can provide a solution for a smaller dark current, the additional cryogenic cooling device reduces the feasibility for lots of applications. Unlike in the infrared regime, imaging in the visible regime can be readily implemented by silicon charged coupled devices (CCDs) with high resolution and high efficiency. Moreover, recent progresses in sensor technology have led to the development of electron multiplying CCDs (EMCCDs) which is capable of single-photon detection. By leveraging the high sensitivity of EMCCDs, ultra-sensitive infrared imaging can be expected with nonlinear frequency upconversion of the infrared electric field to the visible spectral region [10,11]. Here we will introduce a few-photon-level two-dimensional infrared imaging detector by coincidence frequency upconversion. The upconversion imaging apparatus is shown in Fig. 10.

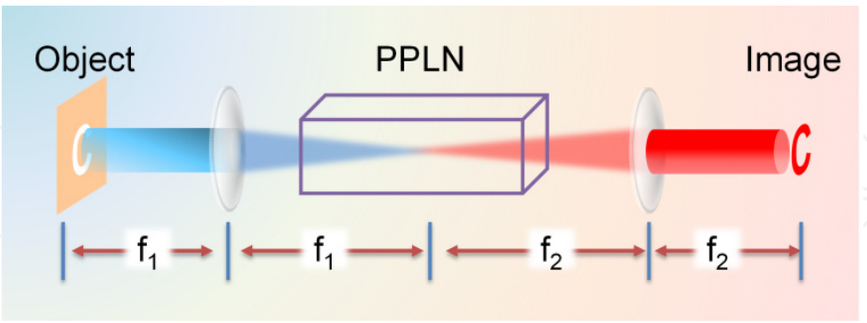

Figure 10. Schematic for infrared imaging by frequency upconversion.

In our experiment, the pump and signal sources were taken from two fiber lasers mode-locked at 19.1 MHz [33]. The signal beam illuminated a transmission mask with a character "C" to form the object beam shown in Fig. 11 (a). By a dichroic mirror, the object beam and the pump beam were then combined into a 4-f imaging system with lens L1 (f_1=250 mm) and L2 (f_2=300 mm). Fourier plane was arranged right at the middle of 50-mm-long PPLN crysta. In order to facilitate the type I quasi-phase matching of the PPLN crystal, a Glan prism was

employed before the crystal for enforcing the polarization [45]. The temperature of the crystal was optimized at 104.3 °C for the grating period of 11.0 μm. The upconverted image at 622 nm was captured by a silicon EMCCD (Andor iXon3 897) bearing 512×512 pixels. The pixel size was 16×16 μm, which was very suitable for high spatial resolution imaging. To improve the signal-to-noise ratio, the EMCCD was thermoelectrically cooled to -85 °C.

With the pump power of 40.0 mW, corresponding to a peak power of about 210 W, the internal conversion efficiency of 27% could be inferred by correcting for the filtering transmittance. The object beam was attenuated to 2.0 photons per pulse. The upconverted imaging photons were then registered by the EMCCD with integration time of 30 s and accumulated for 50 times. The upconverted image was shown in Fig. 11 (c), from which the character "C" could be identified. Thanks to the pulsed pump field together with the long-wavelength pumping, the background noise was remarkably reduced. The theoretical calculation based on coherent imaging theory was given in Fig. 11 (b), which was in good agreement with the experimental result. The image blurring was attributed to the spatial filtering relating to the point spread function in the upconversion imaging system [7]. To improve the resolution, large pump beam profile at the Fourier plane would be better to enwrap the transformed object field as much as possible. However, increasing the diameter of the pump beam would decrease the intensity, thus reduce the conversion efficiency. Thus optimization of the trade-off should be in consideration.

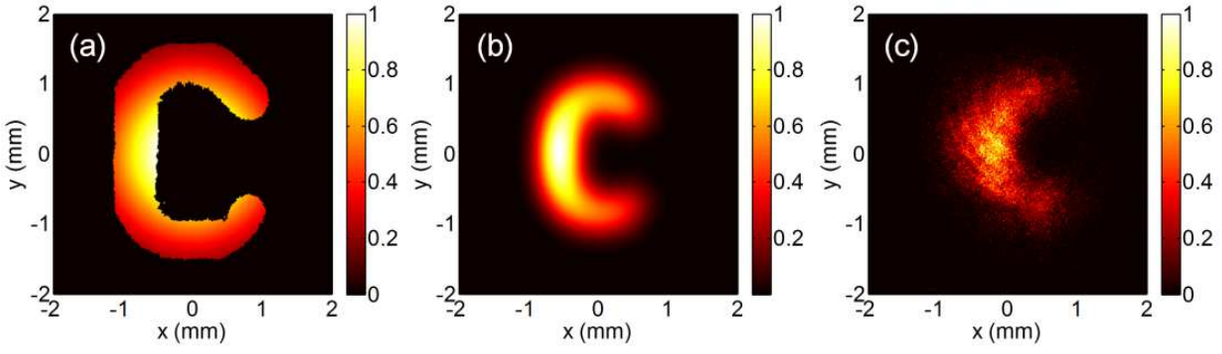

Figure 11. (a) The coherently illuminated mask. The theoretical (b) and measured (c) upconverted images at the image plane.

In summary, we demonstrated full 2D infrared image upconversion at few-photon level with a high conversion efficiency of 31%. The infrared image at 1040 nm was upconverted to the visible regime where the imaging photons were registered by the silicon EMCCD with high sensitivity and resolution. The imaging performance was remarkably improved with the reduction of the background noise by the synchronized pulsed excitation of the 1549 nm pump source, as well as the long-wavelength pumping [46]. Such all-optical upconversion imaging technique can offer an attractive method for ultra-sensitive infrared imaging.

5. Conclusion

In this review chapter, the quantum theory of the frequency upconversion is introduced and indicates that either in single-mode regime and multi-mode regime, complete quantum

transduction can be realized in principle with two necessary requirement, sufficiently intensive pump field and perfect phase matching. Several upconversion systems with high conversion efficiency are presented and discussed in detail. Synchronous pumping frequency upconversion system shows superior performance with high conversion efficiency and low background noise. Thanks to the short time window of the synchronized pump pulse together with long-wavelength pumping scheme, the detection sensitivity was improved remarkably by reducing the background noise. This technique facilitates not only many traditional applications, such as classical optical communication, imaging, photobiology, and astronomy, but also novel quantum optics applications, such as quantum interface to transfer quantum entanglement, linear optical quantum gates, single photon polarization switches, and nonlinear control of single photons.

Author details

Kun Huang, E Wu, Xiaorong Gu, Haifeng Pan and Heping Zeng
State Key Laboratory of Precision Spectroscopy, East China Normal University, China

Acknowledgement

This work was funded in part by National Natural Science Fund of China (10990101, 60907043, 61127014 & 91021014), International Cooperation Projects from Ministry of Science and Technology (2010DFA04410), Key project sponsored by the National Education Ministry of China (109069), Research Fund for the Doctoral Program of Higher Education of China (20090076120024), ECNU Reward for Excellent Doctors in Academics.

6. References

[1] Boyd R (2008) Nonlinear Optics, Academic Press, ISBN 978-0123694706, New York.
[2] Huang J, Kumar P (1992) Observation of Quantum Frequency Conversion. Phys. Rev. Lett. 68: 2153–2156.
[3] Albota M, Wong F (2004) Efficient Single-Photon Counting at 1.55 μm by Means of Frequency Upconversion. Opt. Lett. 29: 1449–1451.
[4] Pan H, Dong H, Zeng H, Lu W (2006) Efficient Single-Photon Counting at 1.55 μm by Intracavity Frequency Upconversion in a Unidirectional Ring Laser. Appl. Phys. Lett. 89: 191108.
[5] Vandevender A, Kwiat P (2004) High Efficiency Single Photon Detection via Frequency Up-Conversion. J. Mod. Opt. 51: 1433–1445.
[6] VanDevender A, Kwiat P (2007) Quantum Transduction via Frequency Upconversion. J. Opt. Soc. Am. B, 24: 295-299.
[7] Pedersen C, Karamehmedović E, Dam J, Tidemand-Lichtenberg P (2009) Enhanced 2D-Image Upconversion Using Solid-State Lasers. Opt. Express 17: 20885-20890.
[8] Kuzucu O, Wong F, Kurimura S, Tovstonog S (2008) Time-Resolved Single-Photon Detection by Femtosecond Upconversion. Opt. Lett. 33: 2257-2259.

[9] Zhang Q, Langrock C, Fejer M, Yamamoto Y (2008) Waveguide-Based Single-Pixel Up-Conversion Infrared Spectrometer. Opt. Express 16: 19557–19561.
[10] Tanzilli S, Tittel W, Halder M, Alibart O, Baldi P, Gisin N, Zbinden H (2005) A Photonic Quantum Information Interface. Nature 437: 116–120.
[11] Rakher M, Ma L, Slattery O, Tang X, Srinivasan K (2010) Quantum Transduction of Telecommunications-Band Single Photons from a Quantum Dot by Frequency Upconversion. Nature Photonics 4: 786–791.
[12] Xu H, Ma L, Mink A, Hershman B, Tang X (2007) 1310-nm Quantum Key Distribution System with Up-Conversion Pump Wavelength at 1550 nm. Opt. Express 15: 7247–7260.
[13] Fejer M, Magel G, Jundt D, Byer R (1992) Quasi-Phase-Matched Second Harmonic Generation: Tuning and Tolerances. IEEE J. Quantum Electron. 28: 2631-2654.
[14] Takesue H, Diamanti E, Langrock C, Fejer M, Yamamoto Y (2006) 1.5 μm Single Photon Counting Using Polarization-Independent Up-conversion Detector. Opt. Express 26: 13067-13072.
[15] Ma L, Slattery O, Tang X (2010) NIR Single Photon Detectors with Up-Conversion Technology and Its Applications in Quantum Communication Systems. InTech. pp. 315–336.
[16] Ramelow S, Fedrizzi A, Poppe A, Langford N, Zeilinger A (2012) Polarization-Entanglement-Conserving Frequency Conversion of Photons. Phys. Rev. A 85: 013845.
[17] Gu X, Huang K, Pan H, Wu E, Zeng H (2012) Photon Correlation in Single-Photon Frequency Upconversion. Opt. Express 20: 2399-2407.
[18] Huang K, Gu X, Ren M, Jian Y, Pan H, Wu G, Wu E, Zeng H (2011) Photon-Number-Resolving Detection at 1.04 μm via Coincidence Frequency Upconversion. Opt. Lett. 36: 1722-1724.
[19] Midwinter J, Warner J (1967) Up-conversion of Near Infrared to Visible Radiation in Lithium-Meta-Niobate, J. Appl. Phys. 38: 519-523.
[20] Kim Y, Kulik S, Shih Y (2001) Quantum Teleportation of A Polarization State with a Complete Bell State Measurement. Phys. Rev. Lett. 86: 1370-1373.
[21] Hum D, Fejer M (2007) Quasi-Phasematching. C. R. Physique 8: 180–198.
[22] Pan H, Zeng H (2006) Efficient and Stable Single-Photon Counting at 1.55 μm by Intracavity Frequency Upconversion. Opt. Lett. 31: 793-795.
[23] Langrock C, Diamanti E, Roussev R, Yamamoto Y, Fejer M, Takesue H (2005) Highly Efficient Single-Photon Detection at Communication Wavelengths by Use of Upconversion in Reverse-Proton-Exchanged Periodically Poled $LiNbO_3$ Waveguides. Opt. Lett. 30: 1725-1727.
[24] Dong H, Pan H, Li Y, Wu E, Zeng H (2008) Efficient Single-Photon Frequency Upconversion at 1.06 μm with Ultralow Background Counts. Appl. Phys. Lett. 93: 071101.
[25] Gu X, Li Y, Pan H, Wu E, Zeng H (2009) High-Speed Single-Photon Frequency Upconversion with Synchronous Pump Pulses. IEEE J. Sel. Top. Quantum Electron. 15: 1748-1752.
[26] Gu X, Huang K, Li Y, Pan H, Wu E, Zeng H (2010) Temporal and Spectral Control of Single-Photon Frequency Upconversion for Pulsed Radiation. Appl. Phys. Lett. 96: 131111.
[27] Huang K, Gu X, Pan H, Wu E, Zeng H (2012) Synchronized Fiber Lasers for Efficient Coincidence Single-Photon Frequency Upconversion. IEEE J. Sel. Top. Quantum Electron. 18: 562-566.

[28] Pan H, Wu E, Dong H, Zeng H (2008) Single-Photon Frequency Up-Conversion with Multimode Pumping. Phys. Rev. A 77: 033815.
[29] Rakher M, Ma L, Davanco M, Slattery O, Tang X, Srinivasan K (2011) Simultaneous Wavelength Translation and Amplitude Modulation of Single Photons from a Quantum Dot. Phys. Rev. Lett. 107: 083602.
[30] Eckstein A, Brecht B, Silberhorn C (2011) A Quantum Pulse Gate Based on Spectrally Engineered Sum Frequency Generation. Opt. Express 19: 13770-13778.
[31] Pomarico E, Sanguinetti B, Thew R, Zbinden H (2010) Room Temperature Photon Number Resolving Detector for Infrared Wavelengths. Opt. Express 18: 10750-10759.
[32] Albota M, Wong F, Shapiro J (2006) Polarization-Independent Frequency Conversion for Quantum Optical Communication. J. Opt. Soc. Am. B 23: 918-924.
[33] Rusu M, Herda R, Okhotnikov O (2004) Passively Synchronized Two-Color Mode-Locked Fiber System Based on Master-Slave Lasers Geometry. Opt. Express 12: 4719-4724.
[34] Hao Q, Li W, Zeng H (2009) High-Power Yb-Doped Fiber Amplification Synchronized with a Few-Cycle Ti: Sapphire Laser. Opt. Express 17: 5815-5821.
[35] Li Y, Gu X, Yan M, Wu E, Zeng H (2009) Square Nanosecond Mode-Locked Er-Fiber Laser Synchronized to a Picosecond Yb-Fiber Laser. Opt. Express 17: 4526-4532.
[36] Xu P, Ji S, Zhu S, Yu X, Sun J, Wang H, He J, Zhu Y, Ming N (2004) Conical Second Harmonic Generation in a Two-Dimensional $\chi^{(2)}$ Photonic Crystal: A Hexagonally Poled $LiTaO_3$ Crystal. Phys. Rev. Lett. 93: 133904.
[37] Allevi A, Bondani M, Andreoni A (2010) Photon-Number Correlations by Photon-Number Resolving Detectors. Opt. Lett. 35: 1707-1709.
[38] Waks E, Diamanti E, Sanders B, Bartlett S, Yamamoto Y (2004) Direct Observation of Nonclassical Photon Statistics in Parametric Down-Conversion. Phys. Rev. Lett. 92: 113602.
[39] Afec I, Natan A, Ambar O, Silberberg Y (2009) Quantum State Measurements Using Multipixel Photon Detectors. Phys. Rev. A 79: 043830.
[40] Eraerds P, Legré M, Rochas A, Zbinden H, Gisin N (2007) SiPM for Fast Photon-Counting and Multiphoton Detection. Opt. Express 15: 14539-14549.
[41] Wu G, Jian Y, Wu E, Zeng H (2009) Photon-Number-Resolving Detection Based on InGaAs/InP Avalanche Photodiode in the Sub-Saturated Mode. Opt. Express 17: 18782-18787.
[42] Honjo T, Takesue H, Kamada H, Nishida Y, Tadanaga O, Asobe M, Inoue K (2007) Long-Distance Distribution of Time-Bin Entangled Photon Pairs over 100 km Using Frequency Up-Conversion Detectors. Opt. Express 15: 13957-13964.
[43] Vasilyev M, Choi S, Kumar P, D'Ariano G (2000) Tomographic Measurement of Joint Photon Statistics of the Twin-Beam Quantum State. Phys. Rev. Lett. 84: 2354–2357.
[44] Liang Y, Jian Y, Chen X, Wu G, Wu E, Zeng H (2011) Room-Temperature Single-Photon Detector Based on InGaAs/InP Avalanche Photodiode with Multichannel Counting Ability. IEEE Photon. Tech. Lett. 23: 115–117.
[45] Thew R, Zbinden H, Gisin N (2008) Tunable Upconversion Photon Detector. Appl. Phys. Lett. 93: 071104.
[46] Pelc J, Zhang Q, Phillips C, Yu L, Yamamoto Y, Fejer M (2012) Cascaded Frequency Upconversion for High-Speed Single-Photon Detection at 1550 nm. Opt. Lett. 37: 476-478.